Journal of Inflammation Research

Dovepress
open access to scientific and medical research

Open Access Full Text Article

ORIGINAL RESEARCH

Transcriptomic Analysis of Cardiac Tissues in a Rodent Model of Coronary Microembolization

Zhaochang Jiang[1], Haohao Lu[2], Beibei Gao[3], Jinyu Huang[3], Yu Ding[4]

[1]Department of Pathology, Second Affiliated Hospital of Zhejiang University, School of Medicine, Hangzhou, Zhejiang, 310009, People's Republic of China; [2]Zhejiang Center of Laboratory Animals, Hangzhou Medical College, Hangzhou, Zhejiang, 310063, People's Republic of China; [3]Department of Cardiology, Hangzhou First People's Hospital, Hangzhou, Zhejiang, 310006, People's Republic of China; [4]Department of Clinical Laboratory, Hangzhou First People's Hospital, Hangzhou, Zhejiang, 310006, People's Republic of China

Correspondence: Yu Ding, Department of Clinical Laboratory, Hangzhou First People's Hospital, Hangzhou, Zhejiang, 310006, People's Republic of China, Email dingyu_zj@126.com

Purpose: Coronary microembolization (CME) can result in cardiac dysfunction, severe arrhythmias, and a reduced coronary flow reserve. Impairment of mitochondrial energy metabolism has been implicated in the progression and pathogenesis of CME; however, its role remains largely undetermined. This study aimed to explore alterations in mitochondria-related genes in CME.

Methods: A rat model of CME was successfully established by injecting plastic microspheres into the left ventricle. The cardiac tissues of the two groups were sequenced and mitochondrial functions were assessed.

Results: Using RNA-Seq, together with GO and KEGG enrichment analyses, we identified 3822 differentially expressed genes (DEGs) in CME rats compared to control rats, and 101 DEGs were mitochondria-related genes. Notably, 36 DEGs were up-regulated and 65 DEGs were down-regulated (CME vs control). In particular, the oxidative phosphorylation (OXPHOS) and mitochondrial electron transport were obviously down-regulated in the CME group. Functional analysis revealed that CME mice exhibited marked reductions in ATP and mitochondrial membrane potential (MMP), by contrast, the production of reactive oxygen species (ROS) was much higher in CME mice than in controls. Protein–protein interaction (PPI) and quantitative PCR (qPCR) validation suggested that eight hub genes including Cmpk2, Isg15, Acsl1, Etfb, Ndufa8, Adhfe1, Gabarapl1 and Acot13 were down-regulated in CME, whereas Aldh18a1 and Hspa5 were up-regulated.

Conclusion: Our findings suggest that dysfunctions in mitochondrial activity and metabolism are important mechanisms for CME, and mitochondria-related DEGs may be potential therapeutic targets for CME.

Keywords: CME, rat model, RNA-Sequence, DEGs, OXPHOS, energy metabolism

Introduction

Coronary microembolization (CME) is a clinical event caused by the rupture of an atherosclerotic plaque in patients with acute coronary syndrome (ACS) and serves as a risk factor for patients undergoing percutaneous coronary intervention (PCI).[1,2] CME can lead to the no-reflow (NR) phenomenon and subsequent adverse cardiac events after PCI, which increases the occurrence of acute myocardial infarction (AMI).[3] Moreover, the local inflammatory response, or notable arrhythmias induced by CME can directly promote myocardial dysfunction, which leads to harmful consequences.[4,5] However, to date, the molecular mechanism and effective treatment for CME remain largely elusive.

During PCI, the incidence of CME varies from 0% to 70%, based on the methods of evaluation.[6] Considering the high incidence and its important role in cardiac mortality, there is an urgent need to investigate the molecular mechanism. Thus, the development of an ideal animal model is critical to explore its potential pathophysiology.

Recently, many studies have confirmed that mitochondrial damage is an important contributor to the progression of the NR phenomenon.[7,8] More importantly, mitochondrion-maintained microcirculation functions via the regulation of the post-ischemic injury signaling pathway, removing the aged and damaged mitochondria via mitophagy, and control of

Received: 17 March 2024
Accepted: 13 September 2024
Published: 23 September 2024

endothelial cells (ECs) survival or death.[9,10] Mitochondrial impairments, such as reductions in mitochondrial metabolism activity and membrane integrity loss are strongly related to exacerbated cardiovascular events.[11]

Previously, we investigated the mechanisms of the cardio-protective effects of Shexiang Tongxin Dropping Pill (STDP), together with Prostaglandin E1 (PGE1) on a CME rat model generated by injecting sodium laurate.[12,13] We found that mice treated with STDP or PGE1 showed markedly reductions in coronary microthrombi; moreover, STDP and PGE1 significantly rescued the activities of antioxidant-related proteins and reversed the impaired mitochondrial functions, inhibited mitochondrial permeability transition pore (mPTP) opening, decreased phosphorylation of AKT-Ser473 and increased phosphorylation of GSK3β-Ser9.[12,13] However, the sodium laurate-induced CME animal model has several limitations; for example, compared with other approaches, animals receiving sodium laurate may manifest relatively severe AMI and inflammation,[14] and sodium laurate may enter the blood circulation and subsequently damage platelets or vascular integrity, thus, causing multiple-organ dysfunction.[15]

In this study, we first generated a rat model by injecting microspheres into the left ventricle. We performed RNA-Sequence analysis of cardiac tissues from the CME and Sham groups (control). We also used KEGG and GO analyses to identify differentially expressed genes (DEGs) between the two groups. The protein–protein interaction (PPI) network of CME was established to screen for hub genes. In addition, we isolated mitochondria from cardiac tissues and verified the role of mitochondrial dysfunction in CME.

Materials and Methods

Animals

Twenty healthy SPF-level Sprague Dawley (SD) mice of both sexes (14–16 weeks old, 350–400g) were obtained from the Zhejiang Center of Laboratory Animals, Hangzhou Medical College [SCXK(Zhe)2019–0002]. Briefly, all mice were housed in a standard animal maintenance facility under a 12-h light–dark cycle in a room maintained at temperature conditions (23±2°C) and 50% relative humidity with free access to water and food. All experimental procedures were conducted according to the National Institute of Health Guild for the Care and Use of Laboratory Animals and were approved by the Experimental Animal Welfare Ethics Committee of the Zhejiang Academy of Medical Sciences (Approval No. ZJCLA-IACUC-20020093).

Establishment of a Mouse Model of CME

Animals were randomly divided into two experimental groups: the CME group (n=10) and sham-operated group (control, n=10). To generate CME model, healthy SD mice were fully anesthetized with 2% inhalation isoflurane (Baxter International Inc., IL, USA) in oxygen and injected with microspheres with a diameter of 42-μm (Biosphere Medical Inc., Rockland, MA) into the left coronary artery, according to a previous study.[16] While another group of animals was administrated saline (0.1-mL intraperitoneal) instead of microspheres. All rats were euthanized by cervical vertebral dislocation 24-h after the operation.

Measurements of Cardiac Functions

Transthoracic echocardiography was performed using Vevo770 ultrasound systems (VisualSonics, Canada) as previously described.[17] Left ventricular ejection fraction (LVEF), left ventricular end-diastolic diameter (LVEDD), left ventricular end-systolic diameter (LVESD), and fractional shortening (FS) were measured according to a previous study.[17] Moreover, the concentrations of plasma atrial natriuretic peptide (ANP) and brain natriuretic peptide (BNP) were analyzed by using commercial ELISA kits (Fine Biotech, Wuhan, China). The heart weight/body weight (HW/BW) ratio was determined as soon as the mice were sacrificed.

Histological Analyses

The heart tissues from three rats in each group were fixed overnight with 4% paraformaldehyde, embedded in paraffin and cut into 5-μm-thick sections. The sections were subsequently stained with hematoxylin and eosin (HE), as described previously.[18]

Transmission Electron Microscopy (TEM) Analysis

Cardiac tissues from three CME mice and three control mice were fixed in glutaraldehyde at 4 °C overnight and then stained with aqueous uranyl acetate for 2-h. All the specimens were pre-infiltrated with propylene oxide, fixed, and embedded in epoxy resin for 48-h. Mouse heart tissues were placed onto copper grids, stained with uranyl acetate, and observed using an HT-7800 TEM (Hitachi, Tokyo) at Zhejiang Center of Laboratory Animals, Hangzhou Medical College, according to a previous study.[19]

RNA-Sequence

Total RNA from three cardiac left-ventricle tissues from each group was extracted using the TRIzol method (Life Technologies, Carlsbad, CA, USA) and stored at −80°C until further use. RNA quality and quantity were assessed using a NanoDrop spectrophotometer (DeNovix DS-11, DE, USA). A specimen RNA Integrity Number (RIN) >7.0 was selected for further experimental analysis. The Illumina TruSeq RNA protocol was used to prepare the library, and RNA-Sequence was analyzed on an Illumina HiSeq 2000 platform (Illumina, San Diego, CA, USA). To obtain high-quality clean reads, low-quality reads or reads containing poly-N were excluded. Gene expression levels were determined using reads per kilobase per million mapped reads (FPKM).

DEGs and Principal Component Analyses (PCA)

Genes with an adjusted p-value <0.05 and $|\log_2(FC)|$ >1.0 were regarded as DEGs. DEGs in both CME and control groups were analyzed by DEseq, based on the method as previously reported.[20] We used GO to perform enrichment analysis on gene sets via the online GOATOOLS (https://github.com/tanghaibao/GOatools).[21] It considered 3 aspects of how DEGs can be described: "biological process"; "cellular component"; and "molecular function". KEGG, a large knowledge base for analyzing gene function, was performed using KOBAS 3.0.[22,23]

In addition, gene set enrichment analysis (GSEA), a bioinformatics tool for determining whether a group of DEGs showed statistical significance between biological samples, and GSEA software (v4.1.0) were used to evaluate the key pathways and core genes during the progression of CME.[24]

PCA is a mathematical algorithm that reduces the dimensionality of the data while retaining most of the variation in the data set,[25] it constructs a set of uncorrelated variables, which correspond to eigenvectors of the sample covariance matrix, according to the method as previously described.[26]

Construction of PPI Network

The PPI network of DEGs was established by using online STRING database (https://string-db.org/cgi/input.pl) and the hub genes were analyzed by Cytoscape (v3.9.1, https://cytoscape.org).[27] When generation of PPI network, we chose the setting option as "Homo sapiens", if a confidence score ≥0.90, it was regarded to be highly trusted.

Quantitative PCR (qPCR) Validation

Total mRNA from the heart tissues of three CME and three control mice was isolated using TRIzol Reagent, as mentioned previously. Subsequently, the PrimeScript™ RT Master Mix (Takara Bio, Shiga, Japan) was used to generate cDNA using an mRNA template. The qPCR assay was run to analyze the expression levels of ten hub genes between the CME and control groups using SYBR Premix Ex Taq (Takara Bio, Shiga) on a CFX96 Touch System (Bio-Rad Laboratories, USA) based on the $2^{-\Delta\Delta Ct}$ method.[28] The primer sequences of ten target genes are displayed in Table 1. All experiments were performed in triplicate.

Analysis of ATP Levels

ATP levels were determined in the heart tissues from the CME and control groups. Experiments were performed using a Luminescence Assay Kit (BioVision Inc. Milpitas) according to the methods provided by manufacturer.[29] All experiments were performed in triplicate.

Table 1 Primer Sequences for qPCR

Gene name	Forward sequence (5'→3')	Reverse sequence (5'→3')
Aldh18a1	ACCTGGATTTCCACGACGAG	GACGGCATCGTTTGTGTTGAC
Cmpk2	TGGGCAATTATCTCGTGGCTT	GCTATGCCAGTACCTGTCTACAA
Isg15	AGTGATGCTAGTGGTACAGAACT	CAGTCTGCGTCAGAAAGACCT
Acsl1	TCTTGGTGTACTACTACGACGAT	CGAGAACCTAAACAAGGACCATT
Etfb	GACTGTAACCAGACAGGTCAGA	CCCGTCAATTTCCCGTTCCA
Hspa5	ACTTGGGGACCACCTATTCCT	GTTGCCCTGATCGTTGGCTA
Ndufa8	GCAGGCAAAGTTTGACCAGTG	GGCAAAGGACGATCTGTTTTCA
Adhfe1	TGACAGACAAGAACCTCTCCC	CATCAAACGCTCCCTTTTTGG
Gabarapl1	AGGACCACCCCTTCGAGTATC	GCACAAGGTACTTCCTCTTATCC
Acot13	GCAACCTTAGTGGACAGCATCTC	CAAGTGTCTTTCCTTGCTTCAGAA
Gapdh	CGTGCCGCCTGGAGAAACC	TGGAAGAGTGGGAGTTGCTGTTG

Mice Cardiac Mitochondria Isolation

Mouse cardiac mitochondria from the two groups were collected on ice by centrifugation at 4 °C, as previously described.[30,31] Protein concentrations were assayed using the BCA method (Thermo Fisher Scientific).

Determining the Levels of Mitochondrial Membrane Potential (MMP) and Reactive Oxygen Species (ROS)

The JC-1 fluorescence (Sigma-Aldrich, Merck KGaA) was used to determine the MMP levels in CME and control rats, as previously described.[32] The microscope reader recorded the green fluorescence of J-monomers (529nm) and red fluorescence of J-aggregates (590nm).[33] While the ROS levels were measured by using 2'-7'-Dichlorodihydrofluorescein diacetate (DCFH-DA), as suggested previously.[34]

Statistical Analysis

Statistical analyses were conducted using SPSS v19.0 and GraphPad Prism v8.0.2. A *t*-test was used to calculate the means of the two groups and detect significance between unpaired samples. Statistically significance was set at p-value <0.05.

Results

Establishment of a Microspheres-Induced CME Rat Model

All the rats in the control group survived without any clinical abnormalities. In CME group, four mice survived after the operation; unfortunately, six mice showed poor performance after the injection of microspheres and died several hours after the operation. Subsequently, we randomly selected three rats from each group for subsequent experiments. As shown in Table 2, echocardiography result indicated that cardiac functions were impaired as characterized by significant decreases in LVEF and FS in the CME group as compared with controls ($p<0.05$ for all). In addition, LVESD, LVEDD, BNP and ANP were increased in CME as compared with control group ($p<0.05$ for all). However, no significant difference was observed in HW/BW and HR between two groups. Furthermore, HE staining showed obvious micro-infarcts around the microspheres in CME mice compared to those in normal rats (Figure 1).

As shown in Figure 2, compared to the control group, TEM of the microvasculature revealed a remarkable impairment of microvascular ECs in CME. For example, the cytoplasm was severely edematous, the organelle structure disappeared and the capillary (cap) wrinkled. However, there was a large-scale disappearance of the basement membrane

Table 2 Comparison of Heart Functions in Rats from CME and Control Groups

Characteristics	Control Group	CME group
HW/BW (mg/g)	3.01±0.14	3.20±0.22
HR (min^{-1})	390±41	400±32
LVESD (mm)	4.09±0.53	4.72±0.78*
LVEDD (mm)	7.23±0.55	7.89±0.37*
LVEF (%)	82.8±5.3	70.6±3.15*
FS (%)	40.5±1.6	23.6±2.6*
BNP (pg/mL)	136±18	255±22*
ANP (pg/mL)	120±10.3	289±17*

Note: *p<0.05.

(BM), which was noticeably thinned. Tight junctions (TJ) were rarely observed, the dense zone was shorter, and intercellular space was locally widened.

As shown in Figure 3, the CME group exhibited moderate degeneration of cardiomyocytes and a relatively severe cellular structure. Furthermore, the organelles showed pronounced swelling, the myofibril filaments were slightly loose and disordered, and the sarcomeres were symmetrically distributed. Importantly, the mitochondria (M) were significantly larger, with moderate swelling, and the membrane was broken. Moreover, the number of sarcoplasmic reticulum (SPR) was significantly reduced, dilated, and vacuoles were changed. Notably, lysosomes (Ly) were present in small amounts and the Z-line (Z) arrangement was disordered, reduced and locally discontinuous. The H-band (H) was arranged locally and disappeared over a large area. These results strongly indicate that microsphere-induced CME causes significant impairment of cardiomyocyte and microvascular functions.

Identification of Common DEGs Between CME and Control Groups

We compared CME and normal heart tissues using RNA-Sequence analysis. Data were filtered using $|\log_2 FC| > 1$ and adjusted to $p < 0.05$. Consequently, 3822 DEGs (CME vs control) were unambiguously identified. A comparison between the two groups suggested that 1919 genes (50.2%) were up-regulated and 1903 genes (49.8%) were down-regulated (Figure 4A and B). The PCA plot is displayed in Figure 4C.

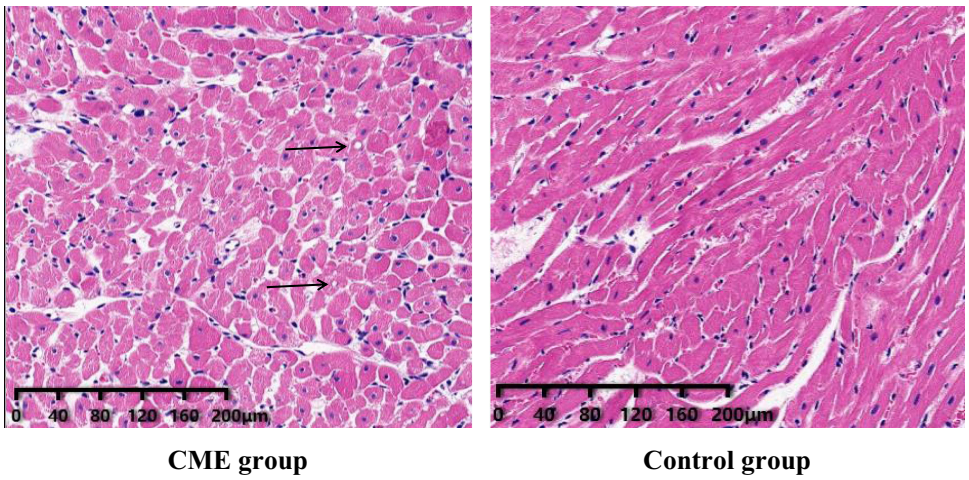

Figure 1 HE staining of myocardial tissues from CME and control groups, arrows indicate the microspheres.

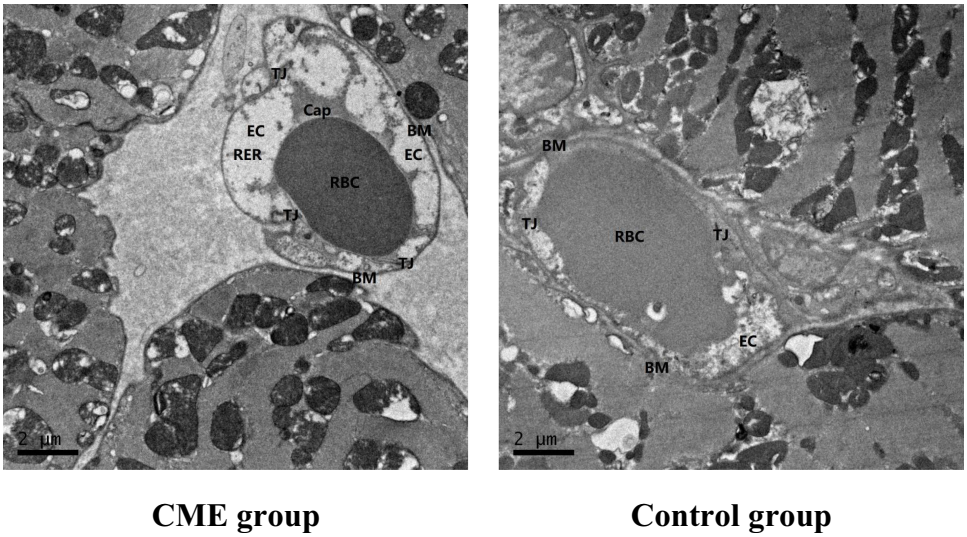

Figure 2 The representative images of ultrastructural changes in mice microvascular from CME and control groups observed under TEM.

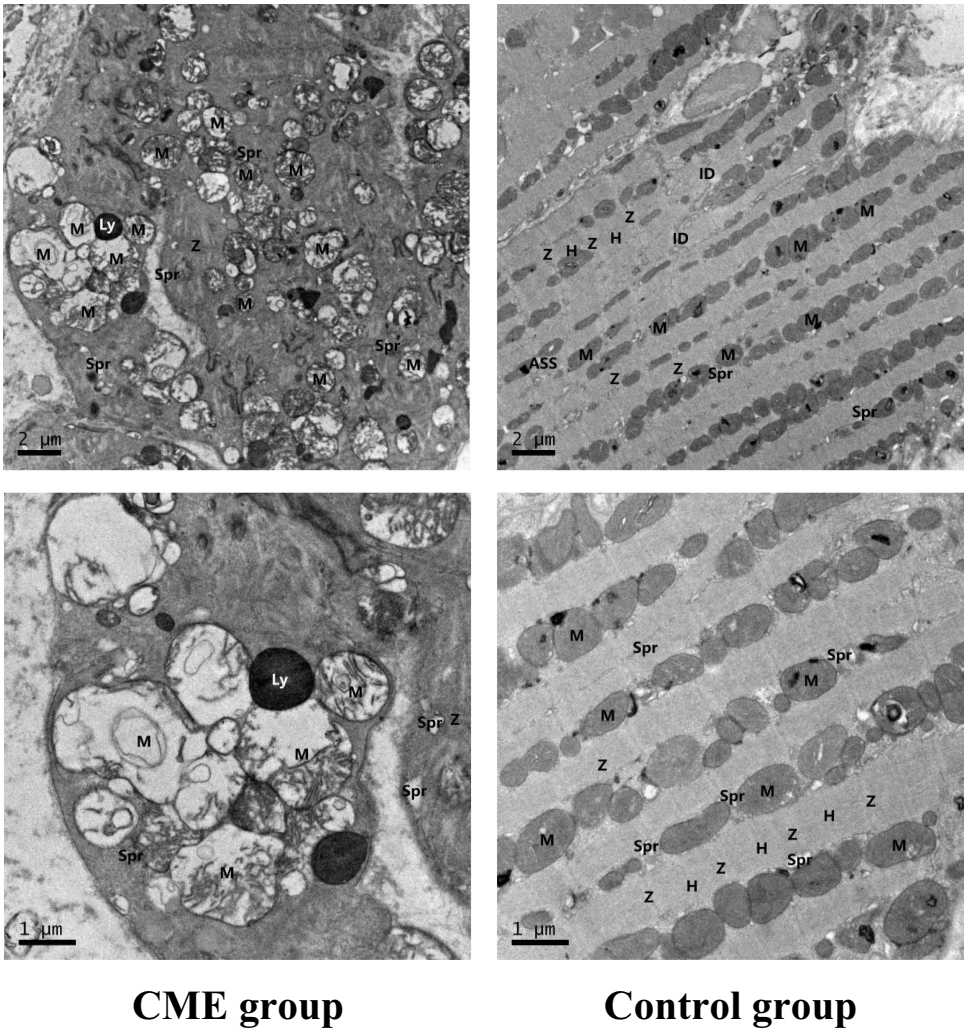

Figure 3 The images of ultrastructural changes in mice cardiomyocyte from CME and control groups observed under TEM.

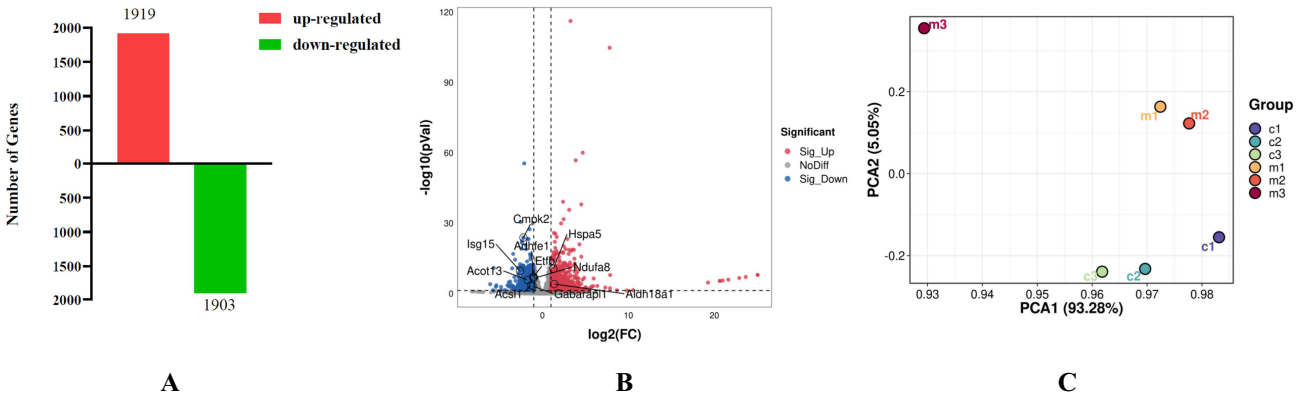

Figure 4 (**A**). Number of upregulated and downregulated genes in CME rats. (**B**). Volcano plot of ten mitochondrial-related DEGs, blue dots indicate the downregulated genes, red dots suggest the upregulated genes. (**C**). A PCA plot for six samples enrolled in RNA-Seq analyses.

Gene Set Analysis

Next, we conducted GO and KEGG enrichment analyses to investigate the potential functions and molecular pathways of the 3822 DEGs. Notably, GO enrichment analysis suggested that these DEGs could be assigned to 20 biological processes, of which the top five of them were mitochondrial respiratory-chain complex I assembly, tricarboxylic acid cycle, mitochondrial electron transport, cytochrome c to oxygen, mitochondrial electron transport, NADH to ubiquinone, and the negative regulation of viral genome replication. In addition, 20 cellular components were significantly enriched, mainly involving the mitochondria, mitochondrial inner membrane, cytoplasm, cytosol, and mitochondrial respiratory-chain complex I. Moreover, significant enrichment was observed in 20 processes related to molecular functions, mainly involving protein binding, identical protein binding, nucleotide binding, oxidoreductase activity and actin filament binding (Figure 5).

Additionally, 20 KEGG pathways were significantly enriched (Figure 6A). Notably, the top five results included pathways involved in diabetic cardiomyopathy, oxidative phosphorylation, Parkinson's disease, thermogenesis, chemical carcinogenesis-reactive oxygen species and non-alcoholic fatty liver disease. According to GO function and KEGG pathway enrichment analyses, mitochondria-related DEGs and oxidative phosphorylation (OXPHOS) signaling pathways were found to be closely related to CME and might play active roles in CME progression. GSEA enrichment analysis also confirmed that a marked decrease in OXPHOS signaling resulting in energy metabolism failure was positively associated with CME, which is consistent with the results of GO and KEGG analyses (Figure 6B).

We further used "heatmap" R package for bidirectional cluster analysis of mitochondria-related DEGs in CME and control groups, the expression levels of 101 DEGs were elaborately and displayed in Figure 7, among which 36 DEGs were up-regulated and 65 DEGs were down-regulated.

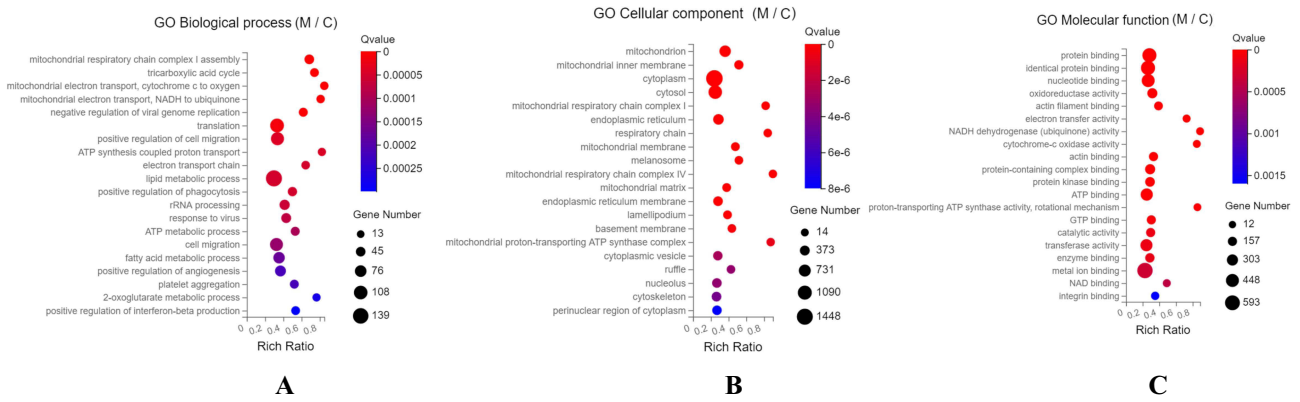

Figure 5 Identification of DEGs in CME, GO enrichment analysis of 101 mitochondria-related DEGs are shown in three functional groups: (**A**). Biological processes of DEGs; (**B**). Cellular component of DEGs; (**C**). Molecular function of DEGs.

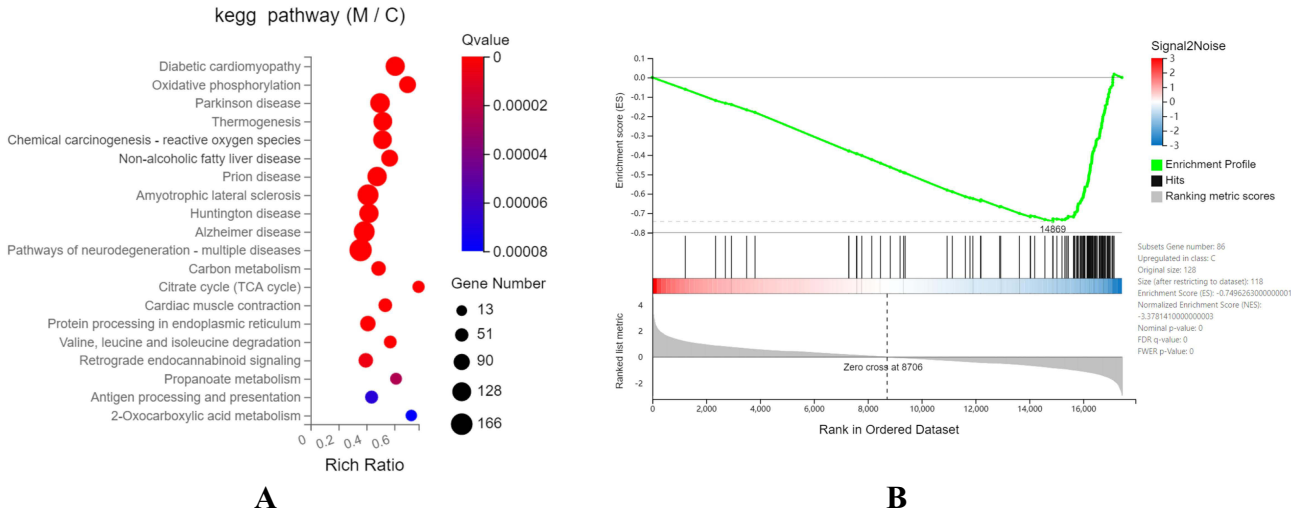

Figure 6 Enrichment analysis of different DEGs in control and CME group. (**A**). KEGG pathway enrichment analysis; (**B**). GSEA functional enrichment analysis of OXPHOS signaling pathway.

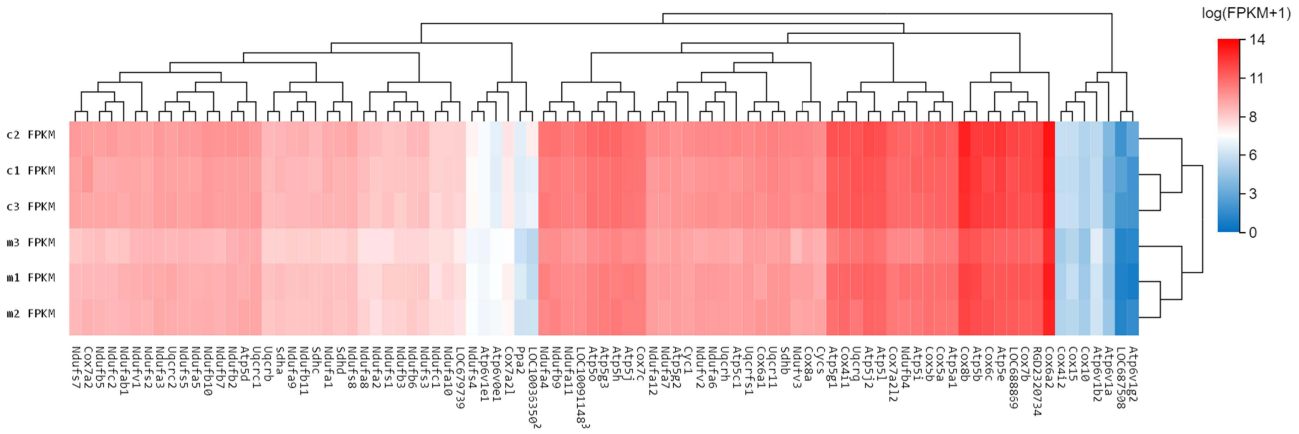

Figure 7 Heatmap of 101 mitochondria-related DEGs in two groups. c: control group, m: CME group.

PPI Analysis

The 101 mitochondria-related nuclear DEGs identified were used to build the PPI network, and the results are shown in Figure 8. Hub genes from the PPI network were screened using the CytoHubba plugin. Based on the maximal clique centrality (MCC) scores, the top ten highest scores for hub genes were as follows: Aldh18a1, Cmpk2, Isg15, Acsl1, Etfb, Hspa5, Ndufa8, Adhfe1, Gabarapl1 and Acot13.

qPCR Analysis

The mRNA expression levels of ten key DEGs involved in mitochondrial energy metabolism were further verified by qPCR. As shown in Figure 9, qPCR revealed that the mRNA levels of Cmpk2, Isg15, Acsl1, Etfb, Ndufa8, Adhfe1, Gabarapl1 and Acot13 in CME were much lower than in the controls ($p<0.05$). However, the transcriptional levels of Aldh18a1 and Hspa5 were significantly higher in the CME rats than in the control rats (all $p<0.001$).

Reduced Mitochondrial Energy Production in CME

Because mitochondria are the main source of ATP generation in cardiomyocytes, defects in OXPHOS function could subsequently lead to impairment of mitochondrial ATP production. As shown in Figure 10, a drastic decrease in MMP

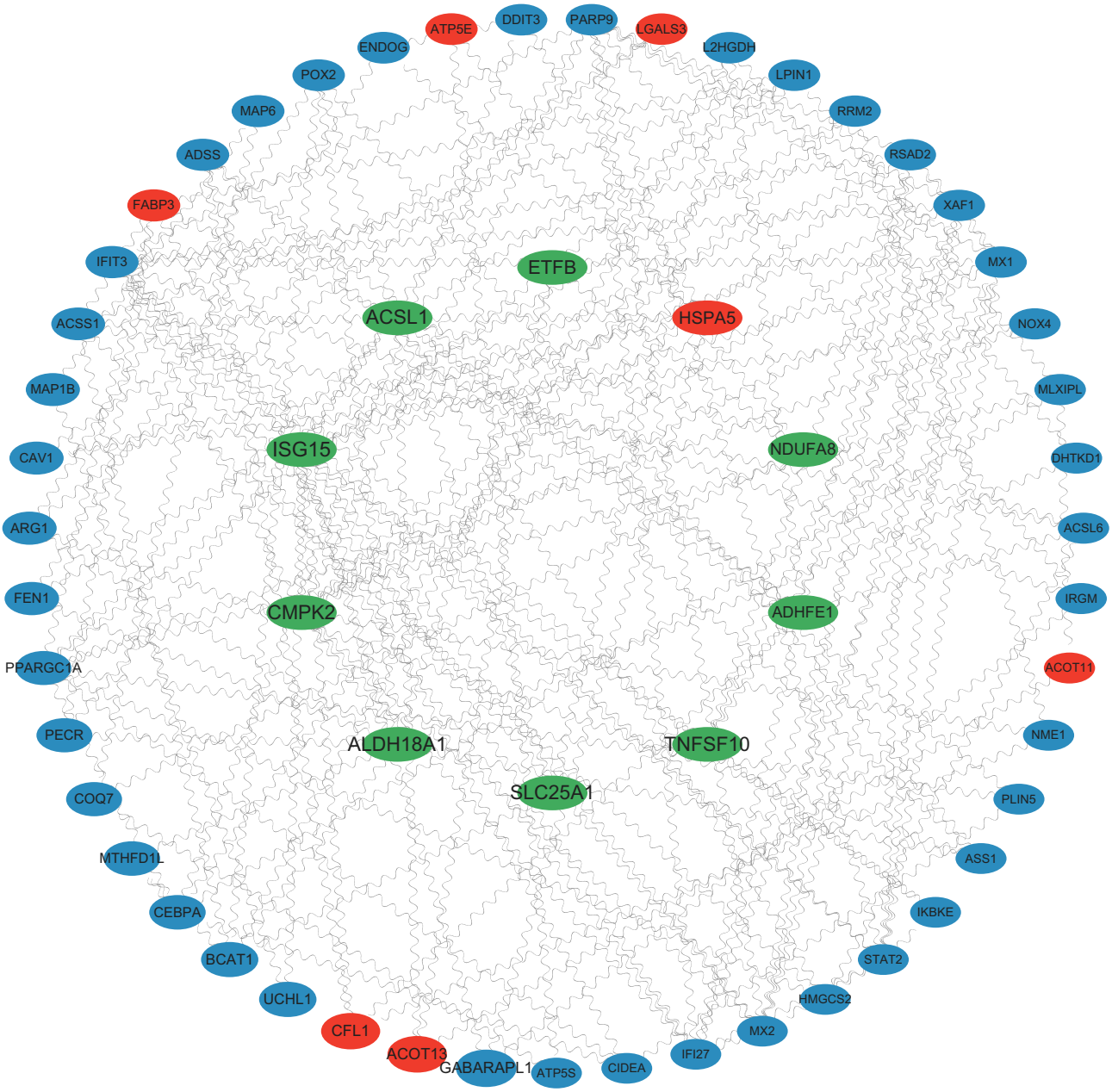

Figure 8 PPI network of mitochondria-related DEGs by using cytoHubba software, the inner circle shows the top 10 high scoring hub genes in CME progression.

and ATP levels in CME rats was observed (p=0.001 and 0.0029, respectively), and a marked increase in ROS production in CME rats was observed compared with control rats (p=0.001).

Discussion

Cardiovascular disease remains a major health problem for both clinicians and scientists. Specifically, CME could worsen cardiac function and lead to severe myocardial fibrosis.[35] It is an important risk factor for poor long-term prognosis among individuals carrying AMI that reduces the coronary circulation.[36] However, it should be noted that mild or moderate CME did not have any clinical symptoms, and only severe CME could lead to NR or even cardiac arrest.[37] Thus, establishing an animal model of CME is critical for understanding its pathophysiology.

Currently, the standard method of generating a CME animal model is the intracoronary injection of microspheres.[38–40] The greatest advantage of using microspheres (diameter: 40-μm) is that the number of injected spheres can be

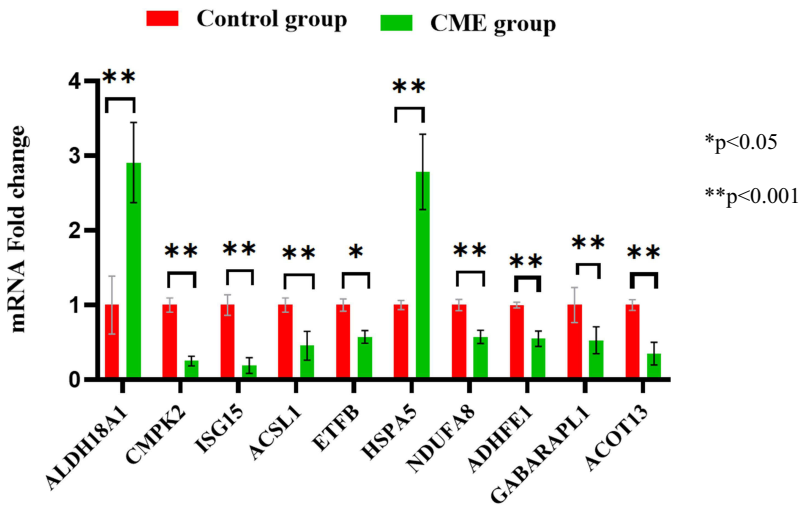

Figure 9 Results of qPCR for the mRNA levels of Aldh18a1, Cmpk2, Isg15, Acsl1, Etfb, Hspa5, Ndufa8, Adhfe1, Gabarapl1 and Acot13 in CME and control groups.

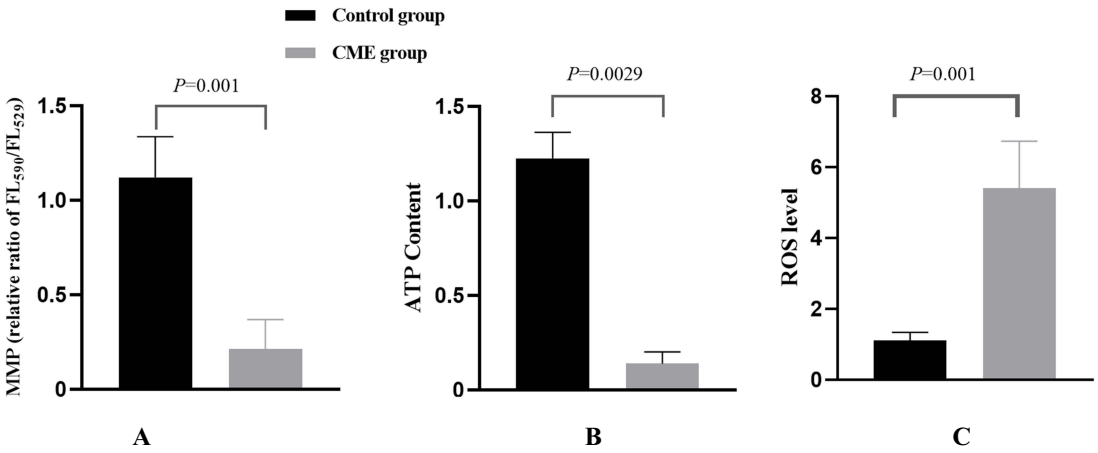

Figure 10 Analysis of mitochondrial functions in CME and control groups. (**A**). MMP analysis; (**B**). determining the ATP level; (**C**). ROS analysis.

standardized to coronary inflow. In addition, mice that received microspheres expressed microinfarcts similar to those reported in AMI patients' hearts, which was consistent with our study, such as evaluated levels of cardiac and mitochondrial dysfunction, remarkable impairment of microvascular ECs, and microinfarction, which was similar to the variable clinical phenotypes of CME.

Mitochondria provide most of the cellular energy to the heart, generating ATP via the electron transport chain. The mitochondrial genome lacks the protection of histones, mitochondrial DNA (mtDNA) is more vulnerable to the accumulation of ROS-induced damage than nuclear DNA.[41] On one hand, dysfunction of OXPHOS systems destroys energy metabolism in ECs. This physiological process caused a large amount of ROS production, increased oxidative stress, and activated inflammatory responses that were involved in CME.[42] Indeed, our study showed significant decreases in MMP and ATP in the CME group, whereas a marked increase in ROS production was observed in CME mice when compared with normal rats ($p<0.05$). Defects in OXPHOS complexes may result in ATP shortage, leading to mitochondrial dysfunction.

We observed that CME mice differentially regulated 3822 genes in the RNA-Sequence datasets. Among these, 101 were mitochondria-related. GO and KEGG pathway enrichment analyses indicated that most of these DEGs were involved in OXPHOS-related pathways. In particular, mitochondrial respiratory-chain complex I assembly, mitochondrial

electron transport, and the inner membrane were strongly related to CME. Furthermore, PPI network analysis revealed that Aldh18a1, Cmpk2, Isg15, Acsl1, Etfb, Hspa5, Ndufa8, Adhfe1, Gabarapl1, and Acot13 are hub genes.

The mouse aldehyde dehydrogenase 18A1 (Aldh18a1) was a bifunctional ATP- and NADPH-dependent mitochondrial enzyme, the encoded protein catalyzed the delta-1-pyrroline-5-carboxylate synthase (P5CS), an important step in the biosynthesis of proline, ornithine and arginine.[43] Mutations in Aldh18a1 were correlated with loss or decrease of P5CS function including proline and the ornithine-derived polyamine, putrescine.[44] Knockdown of Aldh18a1 significantly affected the production of both $NADP^+$ and NADPH.[45] In addition, the Cmpk2, also named UMP-CMP kinase 2, was an enzyme located at mitochondria[46] which played a significant role in pyrimidine metabolism and regulated IFN-α mediated ROS generation.[47] Recent experimental studies revealed that the Cmpk2 linked to LPS-induced mitochondrial biogenesis in bone marrow-derived macrophages (BMDMs) by supplying deoxyribonucleotides.[48] Interestingly, deletion of Cmpk2 impaired mitochondrial-associated metabolic pathways and functions caused mitochondrial deficiency and brain calcification.[49]

The interferon-stimulated gene 15 (Isg15) was highly expressed upon type I interferons treatment to defense against microbial infections.[50] This gene can regulate ubiquitin-like post-translational modification called ISGylation.[51] Importantly, Isg15 and ISGylation were necessary for maintenance of mitochondrial-associated energy metabolism.[52] Previous study suggested that Isg15 governed OXPHOS function during the process of virus infection.[53] Yoshizumi et al[54] reported that mitochondrial normal function was critical for retinoic acid-inducible gene-I-like receptor (RLR)-modulated antiviral signaling, and OXPHOS deficiency rats were more prone to be infected by virus. Juncker et al suggested that Isg15 attenuated congression of impaired mitochondria into mito-aggresomes in Ataxia Telangiectasia (A-T) cells,[55] by contrast, Isg 15 deletion recovered the mitochondrial health in A-T cells. Therefore, Isg 15 may be an important modulator of OXPHOS.

The long-chain acyl-CoA synthetase 1 (Acsl1) was a subtype of the ACSL family that was involved in lipid metabolism.[56] This protein coding gene, however, was located at mitochondrial via the interaction with CTP1b, and was implicated to be involved in mitochondrial fatty acids (FAs) oxidation.[57] Defects in Acsl1 gene in cardiac tissues may lead to an alternation in fuel availability from FA to glucose, subsequently altering the heart functions, impairing OXPHOS functions and promoting the activation of mammalian target of rapamycin complex 1 (mTORC1).[58,59] Furthermore, the electron transfer flavoprotein (ETF) was a nuclear encoded gene which can be imported into mitochondrial and acted as a hub taking up electrons into the OXPHOS system.[60] Mutations in Etfb gene caused the impairment of FA oxidation and mitochondrial-mediated amino acid metabolism.[61,62]

Hspa5, also referred to as BiP or Grp78, belongs to the HSP70 family. It was a mitochondrial-associated endoplasmic reticulum (ER) membrane (MAMs) related protein[63] that involved in regulation of mitochondrial calcium homeostasis, mitophagy and inflammation.[64,65] ER-stress promoted Grp78 localization to mitochondria, which can be further binded to RAF1. In fact, this biological process was important to maintain the mPTP and protected the ER-stress induced apoptosis.[66] Furthermore, the NADH dehydrogenase (ubiquinone) FA8 (Ndufa8) encoded a subunit of OXPHOS Complex I, which was important for proper assembly of this complex.[67] Pathogenic mutations in Ndufa8 gene caused development delay, microcephaly and epilepsy owing to Complex I deficiency.[68–70]

The alcohol dehydrogenase, iron-containing protein 1 (Adhfe1) was a mitochondrial enzyme, which was responsible for catalyzing the gamma-hydroxybutyrate (GHB) to succinic semialdehyde (SSA) coupled to reduction of 2-ketoglutarate (2-KG) to D-2-hydroxyglutarate (D-2-HG).[71] Adhfe1 also played an important role in FAs and iron metabolism.[72,73] The GABA type A receptor associated protein like 1 (Gabarapl1), also referred to as GEC1, was an autophagy-related ubiquitin-like protein family which was involved in autophagosome formation and initiation.[74] Furthermore, the acyl-CoA thioesterase 13 (Acot13), had been suggested to reside on the outer mitochondrial membrane,[75] which played a critical role in hydrolyzing fatty acyl-CoAs to form free FFAs and CoA.[76] In particular, this gene was highly expressed in oxidative tissues, such as liver, heart or kidney.[77] Deletion of Acot13 protected mice against high fat diet-induced hepatic steatosis,[78] emphasizing the significant roles of Acot13 in mitochondrial FA oxidation.

Our results indicated that Cmpk2, Isg15, Acsl1, Etfb, Ndufa8, Adhfe1, Gabarapl1 and Acot13 were down-regulated in CME, whereas Aldh18a1 and Hspa5 were up-regulated as theoretically expected. Because during the progression of

CME, dysfunctions of mitochondrial activities accumulated and impaired the mitochondrial regulated signaling pathways,[79] therefore, genes affecting the mitochondrial OXPHOS functions such as Cmpk2, Isg15, Acsl1, Etfb, Ndufa8, Adhfe1, Gabarapl1 and Acot13 were significantly down-regulated in CME as compared with controls. By contrast, the abnormality of mitochondrial energy metabolism pathway was closely related to CME occurrence; thus, genes located in energy metabolism pathway were significantly overexpressed in CME group. The Aldh18a1 gene, which encoded the P5CS, a key enzyme that linked to glutamate metabolism to proline biosynthesis.[80] In addition, the Hspa5 (Grp78) was present at the mitochondria-associated ER membrane, which was a central hub for all mitochondrial metabolic regulation,[81] thus their expression levels were significantly enhanced in CME group.

In conclusion, using a mice model of CME and transcriptomics analyses technology, we provided the first DEGs characterization of cardiac tissues of CME mice. Bioinformatics analysis revealed a total of 3822 significant DEGs using RNA-Sequence technology (CME vs control). Since the alterations in mitochondrial OXPHOS functions and energy metabolism pathways were the important hallmarks of CME, we finally identified 101 mitochondria-related DEGs that were closely related to CME, of which, ten hub genes (Aldh18a1, Cmpk2, Isg15, Acsl1, Etfb, Hspa5, Ndufa8, Adhfe1, Gabarapl1, and Acot13) played important roles in CME progression. Future studies were warranted to verify if strategies targeting these DEGs and signaling pathways might confer novel therapeutic options for CME or not.

Acknowledgments

We thanked the members of the Department of Cardiology, Hangzhou First People's Hospital for their useful suggestions and comments. This work was supported by grants from Hangzhou Joint Fund of the Zhejiang Provincial Natural Science Foundation of China (No. LHZY24H020002), Zhejiang Provincial Natural Science Foundation of China (No. LQ24H160009), Science Technology of Zhejiang Province (No. 2020C03018), Hangzhou Bureau of Science and Technology (No. 20201203B210 and 20201203B178), and the Hangzhou Municipal Health Commission (No. Z20210019; ZD20220010 and OO20190131).

Author Contributions

All authors made a significant contribution to the work reported, whether that is in the conception, study design, execution, acquisition of data, analysis and interpretation, or in all these areas; took part in drafting, revising or critically reviewing the article; gave final approval of the version to be published; have agreed on the journal to which the article has been submitted; and agree to be accountable for all aspects of the work.

Disclosure

The authors have declared that no competing interests exist.

References

1. Morishima I, Sone T, Okumura K, et al. Angiographic no-reflow phenomenon as a predictor of adverse long-term outcome in patients treated with percutaneous transluminal coronary angioplasty for first acute myocardial infarction. *J Am Coll Cardiol*. 2000;36(4):1202–1209. doi:10.1016/s0735-1097(00)00865-2
2. Heusch G, Kleinbongard P, Böse D, et al. Coronary microembolization: from bedside to bench and back to bedside. *Circulation*. 2009;120(18):1822–1836. doi:10.1161/circulationaha.109.888784
3. Heusch G, Skyschally A, Kleinbongard P. Coronary microembolization and microvascular dysfunction. *Int J Cardiol*. 2018;258:17–23. doi:10.1016/j.ijcard.2018.02.010
4. Falk E, Thuesen L. Pathology of coronary microembolisation and no reflow. *Heart*. 2003;89(9):983–985. doi:10.1136/heart.89.9.983
5. Dörge H, Neumann T, Behrends M, et al. Perfusion-contraction mismatch with coronary microvascular obstruction: role of inflammation. *Am J Physiol*. 2000;279:H2587–92. doi:10.1152/ajpheart.2000.279.6.H2587
6. Heusch G, Schulz R, Haude M, et al. Coronary microembolization. *J Mol Cell Cardiol*. 2004;37(1):23–31. doi:10.1016/j.yjmcc.2004.04.011
7. Zhu H, Toan S, Mui D, et al. Mitochondrial quality surveillance as a therapeutic target in myocardial infarction. *Acta Physiol*. 2021;231(3):e13590. doi:10.1111/apha.13590
8. Bekkers SC, Yazdani SK, Virmani R, et al. Microvascular obstruction: underlying pathophysiology and clinical diagnosis. *J Am Coll Cardiol*. 2010;55(16):1649–1660. doi:10.1016/j.jacc.2009.12.037
9. Chang X, Lochner A, Wang HH, et al. Coronary microvascular injury in myocardial infarction: perception and knowledge for mitochondrial quality control. *Theranostics*. 2021;11(14):6766–6785. doi:10.7150/thno.60143

10. Wu D, Ji H, Du W, et al. Mitophagy alleviates ischemia/reperfusion-induced microvascular damage through improving mitochondrial quality control. *Bioengineered*. 2022;13(2):3596–3607. doi:10.1080/21655979.2022.2027065
11. Miliotis S, Nicolalde B, Ortega M, et al. Forms of extracellular mitochondria and their impact in health. *Mitochondrion*. 2019;48:16–30. doi:10.1016/j.mito.2019.02.002
12. Zhu H, Ding Y, Xu X, et al. Prostaglandin E1 protects coronary microvascular function via the glycogen synthase kinase 3β-mitochondrial permeability transition pore pathway in rat hearts subjected to sodium laurate-induced coronary microembolization. *Am J Transl Res*. 2017;9(5):2520–2534.
13. Ding Y, Zhu HY, Zhang LZ, et al. Shexiang tongxin dropping pill reduces coronary microembolization in rats via regulation of mitochondrial permeability transition pore opening and AKT-GSK3β phosphorylation. *Chin J Integr Med*. 2021;27(7):527–533. doi:10.1007/s11655-019-3176-6
14. Cao YY, Chen ZW, Jia JG, et al. Establishment of a novel mouse model of coronary microembolization. *Chin Med J*. 2016;129(24):2951–2957. doi:10.4103/0366-6999.195469
15. Fang KF, Chen ZJ, Liu M, et al. Blood pH in coronary artery microthrombosis of rats. *Asian Pac J Trop Med*. 2015;8(10):864–869. doi:10.1016/j.apjtm.2015.09.015
16. Su Q, Lv X, Sun Y, et al. Role of TLR4/MyD88/NF-κB signaling pathway in coronary microembolization-induced myocardial injury prevented and treated with nicorandil. *Biomed Pharmacother*. 2018;106:776–784. doi:10.1016/j.biopha.2018.07.014
17. Chen A, Chen Z, Xia Y, et al. Proteomics analysis of myocardial tissues in a mouse model of coronary microembolization. *Front Physiol*. 2018;9:1318. doi:10.3389/fphys.2018.01318
18. Su B, Wang X, Sun Y, et al. miR-30e-3p promotes cardiomyocyte autophagy and inhibits apoptosis via regulating Egr-1 during Ischemia/Hypoxia. *Biomed Res Int*. 2020;2020:7231243. doi:10.1155/2020/7231243
19. Song C, Zhang Y, Pei Q, et al. HSP70 alleviates sepsis-induced cardiomyopathy by attenuating mitochondrial dysfunction-initiated NLRP3 inflammasome-mediated pyroptosis in cardiomyocytes. *Burns Trauma*. 2022;10:tkac043. doi:10.1093/burnst/tkac043
20. Pertea M, Kim D, Pertea GM, et al. Transcript-level expression analysis of RNA-seq experiments with HISAT, stringtie and ballgown. *Nat Protoc*. 2016;11(9):1650–1667. doi:10.1038/nprot.2016.095
21. Klopfenstein DV, Zhang L, Pedersen BS, et al. GOATOOLS: a python library for gene ontology analyses. *Sci Rep*. 2018;8(1):10872. doi:10.1038/s41598-018-28948-z
22. Kanehisa M, Goto S. KEGG: Kyoto encyclopedia of genes and genomes. *Nucleic Acids Res*. 2000;28(1):27–30. doi:10.1093/nar/28.1.27
23. Wu J, Mao X, Cai T, et al. KOBAS server: a web-based platform for automated annotation and pathway identification. *Nucleic Acids Res*. 2006;34(Web Server):W720–4. doi:10.1093/nar/gkl167
24. Subramanian A, Tamayo P, Mootha VK, et al. Gene set enrichment analysis: a knowledge-based approach for interpreting genome-wide expression profiles. *Proc Natl Acad Sci U S A*. 2005;102(43):15545–15550. doi:10.1073/pnas.0506580102
25. Ringnér M. What is principal component analysis? *Nat Biotechnol*. 2008;26(3):303–304. doi:10.1038/nbt0308-303
26. Chen X, Zhang B, Wang T, et al. Robust principal component analysis for accurate outlier sample detection in RNA-Seq data. *BMC Bioinf*. 2020;21(1):269. doi:10.1186/s12859-020-03608-0
27. von Mering C, Huynen M, Jaeggi D, et al. STRING: a database of predicted functional associations between proteins. *Nucleic Acids Res*. 2003;31(1):258–261. doi:10.1093/nar/gkg034
28. Livak KJ, Schmittgen TD. Analysis of relative gene expression data using real-time quantitative PCR and the 2(-Delta Delta C(T)) Method. *Methods*. 2001;25(4):402–408. doi:10.1006/meth.2001.1262
29. Jouaville LS, Pinton P, Bastianutto C, et al. Regulation of mitochondrial ATP synthesis by calcium: evidence for a long-term metabolic priming. *Proc Natl Acad Sci U S A*. 1999;96(24):13807–13812. doi:10.1073/pnas.96.24.13807
30. Kamath VG, Hsiung CH, Lizenby ZJ, et al. Heart mitochondrial TTP synthesis and the compartmentalization of TMP. *J Biol Chem*. 2015;290(4):2034–2041. doi:10.1074/jbc.M114.624213
31. McCann KA, Williams DW, McKee EE. Metabolism of deoxypyrimidines and deoxypyrimidine antiviral analogs in isolated brain mitochondria. *J Neurochem*. 2012;122(1):126–137. doi:10.1111/j.1471-4159.2012.07765.x
32. Bao Y, Wang X, Li W, et al. 20-Hydroxyeicosatetraenoic acid induces apoptosis in neonatal rat cardiomyocytes through mitochondrial-dependent pathways. *J Cardiovasc Pharmacol*. 2011;57(3):294–301. doi:10.1097/FJC.0b013e3182073c78
33. Yuan Y, Chen Y, Zhang P, et al. Mitochondrial dysfunction accounts for aldosterone-induced epithelial-to-mesenchymal transition of renal proximal tubular epithelial cells. *Free Radic Biol Med*. 2012;53(1):30–43. doi:10.1016/j.freeradbiomed.2012.03.015
34. Eruslanov E, Kusmartsev S. Identification of ROS using oxidized DCFDA and flow-cytometry. *Methods Mol Biol*. 2010;594:57–72. doi:10.1007/978-1-60761-411-1_4
35. de Waha S, Patel MR, Granger CB, et al. Relationship between microvascular obstruction and adverse events following primary percutaneous coronary intervention for ST-segment elevation myocardial infarction: an individual patient data pooled analysis from seven randomized trials. *Eur Heart J*. 2017;38(47):3502–3510. doi:10.1093/eurheartj/ehx414
36. Jaffe R, Charron T, Puley G, et al. Microvascular obstruction and the no-reflow phenomenon after percutaneous coronary intervention. *Circulation*. 2008;117(24):3152–3156. doi:10.1161/CIRCULATIONAHA.107.742312
37. Su Q, Lv X, Ye Z. Ligustrazine attenuates myocardial injury induced by coronary microembolization in rats by activating the PI3K/Akt pathway. *Oxid Med Cell Longev*. 2019;2019:6791457. doi:10.1155/2019/6791457
38. Li L, Zhao X, Lu Y, et al. Altered expression of pro- and anti-inflammatory cytokines is associated with reduced cardiac function in rats following coronary microembolization. *Mol Cell Biochem*. 2010;342(1–2):183–190. doi:10.1007/s11010-010-0482-x
39. Carlsson M, Wilson M, Martin AJ, et al. Myocardial microinfarction after coronary microembolization in swine: MR imaging characterization. *Radiology*. 2009;250(3):703–713. doi:10.1148/radiol.2503081000
40. Thielmann M, Dörge H, Martin C, et al. Myocardial dysfunction with coronary microembolization: signal transduction through a sequence of nitric oxide, tumor necrosis factor-alpha, and sphingosine. *Circ Res*. 2002;90(7):807–813. doi:10.1161/01.res.0000014451.75415.36
41. Ballinger SW, Patterson C, Yan CN, et al. Hydrogen peroxide- and peroxynitrite-induced mitochondrial DNA damage and dysfunction in vascular endothelial and smooth muscle cells. *Circ Res*. 2000;86(9):960–966. doi:10.1161/01.res.86.9.960
42. Dromparis P, Sutendra G, Michelakis ED. The role of mitochondria in pulmonary vascular remodeling. *J Mol Med*. 2010;88(10):1003–1010. doi:10.1007/s00109-010-0670-x

43. Hu CA, Khalil S, Zhaorigetu S, et al. Human Delta1-pyrroline-5-carboxylate synthase: function and regulation. *Amino Acids*. 2008;35(4):665–672. doi:10.1007/s00726-008-0075-0
44. Colonna MB, Moss T, Mokashi S, et al. Functional assessment of homozygous ALDH18A1 variants reveals alterations in amino acid and antioxidant metabolism. *Hum Mol Genet*. 2023;32(5):732–744. doi:10.1093/hmg/ddac226
45. Liu W, Hancock CN, Fischer JW, et al. Proline biosynthesis augments tumor cell growth and aerobic glycolysis: involvement of pyridine nucleotides. *Sci Rep*. 2015;5(1):17206. doi:10.1038/srep17206
46. Xu Y, Johansson M, Karlsson A. Human UMP-CMP kinase 2, a novel nucleoside monophosphate kinase localized in mitochondria. *J Biol Chem*. 2008;283(3):1563–1571. doi:10.1074/jbc.M707997200
47. Lai JH, Hung LF, Huang CY, et al. Mitochondrial protein CMPK2 regulates IFN alpha-enhanced foam cell formation, potentially contributing to premature atherosclerosis in SLE. *Arthritis Res Ther*. 2021;23(1):120. doi:10.1186/s13075-021-02470-6
48. Zhong Z, Liang S, Sanchez-Lopez E, et al. New mitochondrial DNA synthesis enables NLRP3 inflammasome activation. *Nature*. 2018;560 (7717):198–203. doi:10.1038/s41586-018-0372-z
49. Zhao M, Su HZ, Zeng YH, et al. Loss of function of CMPK2 causes mitochondria deficiency and brain calcification. *Cell Discov*. 2022;8(1):128. doi:10.1038/s41421-022-00475-2
50. Li C, Wang J, Zhang H, et al. Interferon-stimulated gene 15 (ISG15) is a trigger for tumorigenesis and metastasis of hepatocellular carcinoma. *Oncotarget*. 2014;5(18):8429–8441. doi:10.18632/oncotarget.2316
51. Zhang D, Zhang DE. Interferon-stimulated gene 15 and the protein ISGylation system. *J Interferon Cytokine Res*. 2011;31(1):119–130. doi:10.1089/jir.2010.0110
52. Alcalá S, Sancho P, Martinelli P, et al. ISG15 and ISGylation is required for pancreatic cancer stem cell mitophagy and metabolic plasticity. *Nat Commun*. 2020;11(1):2682. doi:10.1038/s41467-020-16395-2
53. Baldanta S, Fernández-Escobar M, Acín-Perez R, et al. ISG15 governs mitochondrial function in macrophages following vaccinia virus infection. *PLoS Pathog*. 2017;13(10):e1006651. doi:10.1371/journal.ppat.1006651
54. Yoshizumi T, Imamura H, Taku T, et al. RLR-mediated antiviral innate immunity requires oxidative phosphorylation activity. *Sci Rep*. 2017;7 (1):5379. doi:10.1038/s41598-017-05808-w
55. Juncker M, Kim C, Reed R, et al. ISG15 attenuates post-translational modifications of mitofusins and congression of damaged mitochondria in ataxia telangiectasia cells. *Biochim Biophys Acta Mol Basis Dis*. 2021;1867(6):166102. doi:10.1016/j.bbadis.2021.166102
56. Zeng S, Wu F, Chen M, et al. Inhibition of fatty acid translocase (FAT/CD36) palmitoylation enhances hepatic fatty acid β-oxidation by increasing its localization to mitochondria and interaction with long-chain Acyl-CoA synthetase 1. *Antioxid Redox Signal*. 2022;36(16–18):1081–1100. doi:10.1089/ars.2021.0157
57. Han Y, Yan J, Li ZY, et al. Cyclic stretch promotes vascular homing of endothelial progenitor cells via Acsl1 regulation of mitochondrial fatty acid oxidation. *Proc Natl Acad Sci U S A*. 2023;120:e2219630120. doi:10.1073/pnas.2219630120
58. Grevengoed TJ, Cooper DE, Young PA, et al. Loss of long-chain acyl-CoA synthetase isoform 1 impairs cardiac autophagy and mitochondrial structure through mechanistic target of rapamycin complex 1 activation. *FASEB J*. 2015;29(11):4641–4653. doi:10.1096/fj.15-272732
59. Grevengoed TJ, Martin SA, Katunga L, et al. Acyl-CoA synthetase 1 deficiency alters cardiolipin species and impairs mitochondrial function. *J Lipid Res*. 2015;56(8):1572–1582. doi:10.1194/jlr.M059717
60. Henriques BJ, Katrine Jentoft Olsen R, Gomes CM, et al. Electron transfer flavoprotein and its role in mitochondrial energy metabolism in health and disease. *Gene*. 2021;776:145407. doi:10.1016/j.gene.2021.145407
61. Olsen RK, Andresen BS, Christensen E, et al. Clear relationship between ETF/ETFDH genotype and phenotype in patients with multiple acyl-CoA dehydrogenation deficiency. *Hum Mutat*. 2003;22(1):12–23. doi:10.1002/humu.10226
62. Colombo I, Finocchiaro G, Garavaglia B, et al. Mutations and polymorphisms of the gene encoding the beta-subunit of the electron transfer flavoprotein in three patients with glutaric acidemia type II. *Hum Mol Genet*. 1994;3(3):429–435. doi:10.1093/hmg/3.3.429
63. Ni M, Lee AS. ER chaperones in mammalian development and human diseases. *FEBS Lett*. 2007;581(19):3641–3651. doi:10.1016/j.febslet.2007.04.045
64. Yan Z, Kronemberger A, Blomme J, et al. Exercise leads to unfavourable cardiac remodelling and enhanced metabolic homeostasis in obese mice with cardiac and skeletal muscle autophagy deficiency. *Sci Rep*. 2017;7(1):7894. doi:10.1038/s41598-017-08480-2
65. Xiao Y, Chen W, Zhong Z, et al. Electroacupuncture preconditioning attenuates myocardial ischemia-reperfusion injury by inhibiting mitophagy mediated by the mTORC1-ULK1-FUNDC1 pathway. *Biomed Pharmacother*. 2020;127:110148. doi:10.1016/j.biopha.2020.110148
66. Shu CW, Sun FC, Cho JH, et al. GRP78 and Raf-1 cooperatively confer resistance to endoplasmic reticulum stress-induced apoptosis. *J Cell Physiol*. 2008;215(3):627–635. doi:10.1002/jcp.21340
67. Stroud DA, Surgenor EE, Formosa LE, et al. Accessory subunits are integral for assembly and function of human mitochondrial complex I. *Nature*. 2016;538(7623):123–126. doi:10.1038/nature19754
68. Triepels R, van den Heuvel L, Loeffen J, et al. The nuclear-encoded human NADH: ubiquinone oxidoreductase NDUFA8 subunit: cDNA cloning, chromosomal localization, tissue distribution, and mutation detection in complex-I-deficient patients. *Hum Genet*. 1998;103(5):557–563. doi:10.1007/s004390050869
69. Yatsuka Y, Kishita Y, Formosa LE, et al. A homozygous variant in NDUFA8 is associated with developmental delay, microcephaly, and epilepsy due to mitochondrial complex I deficiency. *Clin Genet*. 2020;98(2):155–165. doi:10.1111/cge.13773
70. Tort F, Barredo E, Parthasarathy R, et al. Biallelic mutations in NDUFA8 cause complex I deficiency in two siblings with favorable clinical evolution. *Mol Genet Metab*. 2020;131(3):349–357. doi:10.1016/j.ymgme.2020.10.005
71. Deng Y, Wang Z, Gu S, et al. Cloning and characterization of a novel human alcohol dehydrogenase gene (ADHFe1). *DNA Seq*. 2002;13 (5):301–306. doi:10.1080/1042517021000011636
72. Lyon RC, Johnston SM, Panopoulos A, et al. Enzymes involved in the metabolism of gamma-hydroxybutyrate in SH-SY5Y cells: identification of an iron-dependent alcohol dehydrogenase ADHFe1. *Chem Biol Interact*. 2009;178(1–3):283–287. doi:10.1016/j.cbi.2008.10.025
73. Kim JY, Tillison KS, Zhou S, et al. Differentiation-dependent expression of Adhfe1 in adipogenesis. *Arch Biochem Biophys*. 2007;464(1):100–111. doi:10.1016/j.abb.2007.04.018
74. Jacquet M, Guittaut M, Fraichard A, et al. The functions of Atg8-family proteins in autophagy and cancer: linked or unrelated? *Autophagy*. 2021;17 (3):599–611. doi:10.1080/15548627.2020.1749367

75. Tillander V, Alexson SEH, Cohen DE. Deactivating fatty acids: acyl-CoA thioesterase-mediated control of lipid metabolism. *Trends Endocrinol Metab*. 2017;28(7):473–484. doi:10.1016/j.tem.2017.03.001
76. Cooper DE, Young PA, Klett EL, et al. Physiological consequences of compartmentalized Acyl-CoA metabolism. *J Biol Chem*. 2015;290 (33):20023–20031. doi:10.1074/jbc.R115.663260
77. Wei J, Kang HW, Cohen DE. Thioesterase superfamily member 2 (Them2)/acyl-CoA thioesterase 13 (Acot13): a homotetrameric hotdog fold thioesterase with selectivity for long-chain fatty acyl-CoAs. *Biochem J*. 2009;421(2):311–322. doi:10.1042/BJ20090039
78. Kang HW, Niepel MW, Han S, et al. Thioesterase superfamily member 2/acyl-CoA thioesterase 13 (Them2/Acot13) regulates hepatic lipid and glucose metabolism. *FASEB J*. 2012;26(5):2209–2221. doi:10.1096/fj.11-202853
79. Zhou H, Toan S. Pathological roles of mitochondrial oxidative stress and mitochondrial dynamics in cardiac microvascular ischemia/reperfusion injury. *Biomolecules*. 2020;10(1):85. doi:10.3390/biom10010085
80. Cui C, Wang J, Guo L, et al. PINCH-1 promotes Δ1-pyrroline-5-carboxylate synthase expression and contributes to proline metabolic reprogramming in lung adenocarcinoma. *Amino Acids*. 2021;53(12):1875–1890. doi:10.1007/s00726-021-03050-3
81. Prasad M, Pawlak KJ, Burak WE, et al. Mitochondrial metabolic regulation by GRP78. *Sci Adv*. 2017;3(2):e1602038. doi:10.1126/sciadv.1602038